

# Anti-arrhythmic Medication Propafenone a Potential Drug for Alzheimer's Disease Inhibiting Aggregation of A $\beta$ : In Silico and in Vitro Studies

Son Tung Ngo,<sup>†,‡,§</sup> Shang-Ting Fang,<sup>§,†</sup> Shu-Hsiang Huang,<sup>§</sup> Chao-Liang Chou,<sup>§,||,⊥</sup>  
Pham Dinh Quoc Huy,<sup>†,‡</sup> Mai Suan Li,<sup>\*,‡</sup> and Yi-Cheng Chen<sup>\*,§</sup>

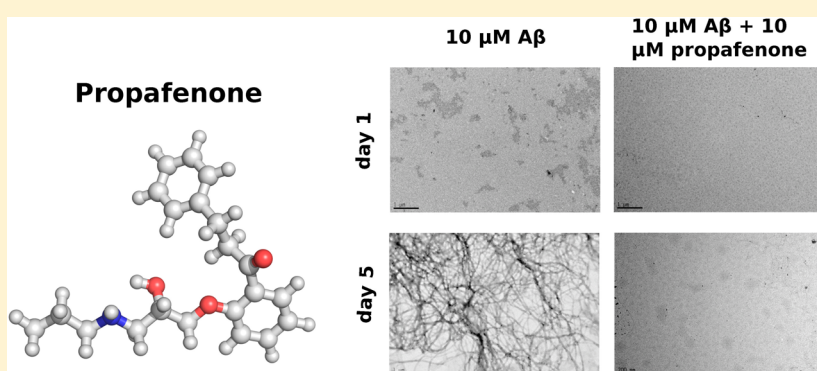
<sup>†</sup>Institute for Computational Science and Technology, Quang Trung Software City, Tan Chanh Hiep Ward, District 12, Ho Chi Minh City, Vietnam

<sup>‡</sup>Institute of Physics, Polish Academy of Sciences, Al. Lotnikow 32/46, 02-668 Warsaw, Poland

<sup>§</sup>Department of Medicine, <sup>||</sup>Institute of Biomedical Sciences, MacKay Medical College, New Taipei City, 252 Taiwan

<sup>\*</sup>Department of Neurology, Mackay Memorial Hospital, New Taipei City, 252 Taiwan

## Supporting Information



**ABSTRACT:** Alzheimer's disease (AD) is the most common form of dementia caused by the formation of A $\beta$  aggregates. So far, no effective medicine for the treatment of AD is available. Many efforts have been made to find effective medicine to cope with AD. Curcumin is a drug candidate for AD, being a potent anti-amyloidogenic compound, but the results of clinical trials for it were either negative or inclusive. In the present study, we took advantages from accumulated knowledge about curcumin and have screened out four compounds that have chemical and structural similarity with curcumin more than 80% from all FDA-approved oral drugs. Using all-atom molecular dynamics simulation and the free energy perturbation method we showed that among predicted compounds anti-arrhythmic medication propafenone shows the best anti-amyloidogenic activity. The in vitro experiment further revealed that it can inhibit A $\beta$  aggregation and protect cells against A $\beta$  induced cytotoxicity to almost the same extent as curcumin. Our results suggest that propafenone may be a potent drug for the treatment of Alzheimer's disease.

## INTRODUCTION

Alzheimer's disease (AD) is a neurodegenerative disorder mainly observed among the senior population.<sup>1,2</sup> As AD progresses, the memory and cognitive function of patients slowly deteriorates.<sup>3–5</sup> Recently, many experiments have demonstrated that AD is associated with aggregation of  $\beta$ -amyloid (A $\beta$ ) peptides which mainly consist of 40 (A $\beta$ <sub>40</sub>) and 42 (A $\beta$ <sub>42</sub>) amino acids.<sup>6,7</sup> Intrinsically disordered A $\beta$  peptides may misfold into amyloid aggregates, including oligomer and fibril, and produce cytotoxicity.<sup>6</sup> With this information, it follows that one can prevent AD by inhibiting A $\beta$  aggregation.<sup>7</sup>

There are several strategies to design new inhibitors for A $\beta$ . One of them is to search candidates among compounds which are available in databases but with unknown pharmaceutical properties for A $\beta$  activity. Along this category, potential A $\beta$  inhibitors have been discovered including short  $\beta$ -sheet breaker

peptides,<sup>8–10</sup> natural compounds,<sup>11–14</sup> vitamin K3 derivatives,<sup>15</sup> etc. The second strategy is to find potential candidates among FDA approved drugs.<sup>16</sup> For instance, adenosine triphosphate,<sup>17</sup> carvedilol,<sup>18</sup> and nilvadipine<sup>19</sup> are under clinical trials as potential inhibitors for A $\beta$  aggregation.<sup>20–22</sup> The third strategy is to screen out compounds that have high similarity with well-known inhibitors.<sup>23</sup> One of those antiamyloidogenic compounds, curcumin has been extensively studied. With in vitro and in vivo studies, curcumin has been demonstrated to protect cells against A $\beta$  induced cytotoxicity, to prevent A $\beta$  fibril formation, to reduce inflammation and oxidative stress, to decrease the A $\beta$  plaques and oligomers in mouse models, and to restore cognitive function.<sup>13,14,24–26</sup> Furthermore, few

**Received:** January 22, 2016

**Published:** June 15, 2016



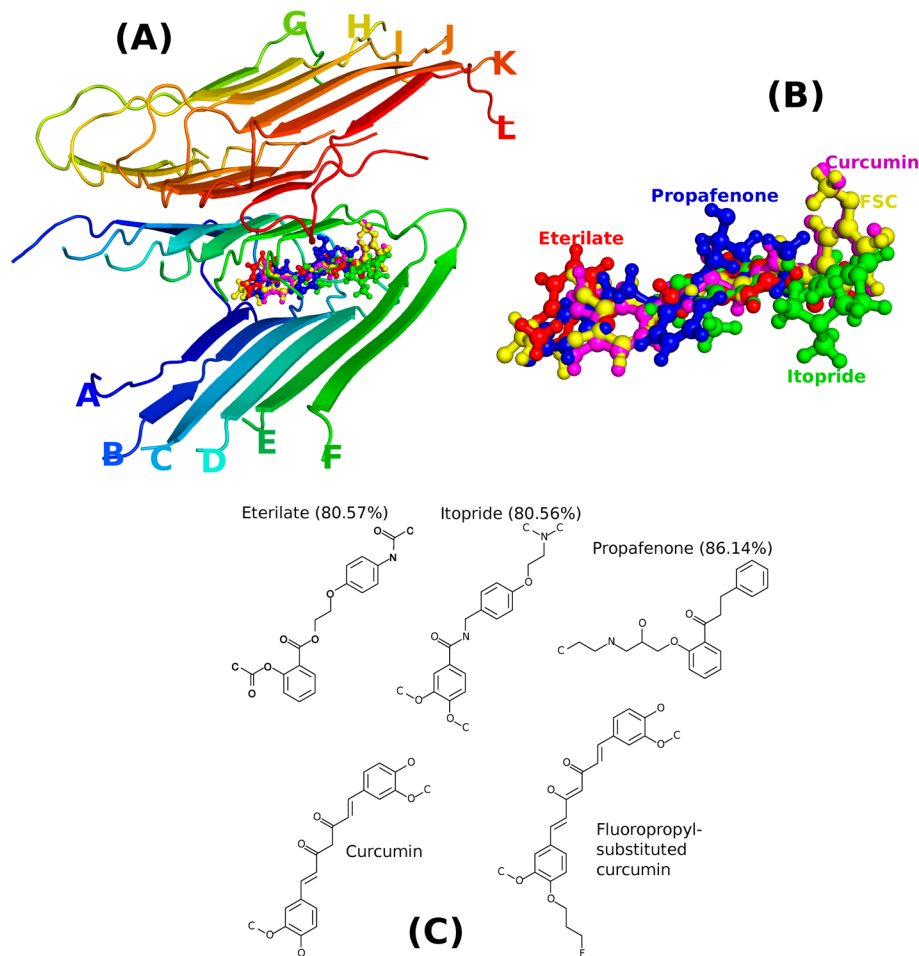


**Figure 1.** (A) Structures and binding poses of five ligands to 2-fold 12  $\text{A}\beta_{9-40}$  peptide. The conformations of complexes were obtained in the best docking mode with the lowest binding energy. These conformations were used as starting conformations for MD simulation. Peptides from the lower and upper layer are denoted by letters A–F and G–L, respectively. (B) Superimposition of five ligands in the best docking mode (enlarged version of the part shown in A). (C) Chemical structure of five ligands. Similarities with curcumin are 80.57, 80.56, and 86.14% for eterilate, itopride, and propafenone, respectively.

clinical trials to evaluate the safety and tolerability of curcumin in AD patients have been conducted.<sup>27,28</sup> However, according to the results of the completed cases, the effect of curcumin on AD were negative or inconclusive.<sup>27,28</sup>

Here we combine the second and third strategies to search potential drugs for treatment of AD. Since curcumin is prominent in blocking  $\text{A}\beta$  aggregation,<sup>14</sup> we narrow down our search to those FDA approved drugs that have high chemical and structural similarity with curcumin. Using QikProp implemented in the Schrodinger package,<sup>29</sup> we have found eterilate, itopride, and propafenone which have more than 80% similarity with curcumin (Figure 1B). A QSAR (quantitative structure–activity relationship) study on the capability of propafenone in inhibiting  $\text{A}\beta$  peptides was conducted,<sup>30</sup> but the nature of its binding to  $\text{A}\beta$  peptide has not been examined by all-atom molecular dynamics (MD) simulation and experiment. Fluoropropyl-substituted curcumin (FSC), synthesized by Ryu et al.,<sup>31</sup> is a strong inhibitor of  $\text{A}\beta$  aggregation as it has very low inhibition constant  $K_i = 0.07 \text{ nM}$ . However, the binding mechanism of FSC to  $\text{A}\beta$  peptide has not been studied at atomic level.

Using the docking and free energy perturbation (FEP) methods,<sup>32–34</sup> we have found that propafenone has the highest binding affinity to  $\text{A}\beta_{40}$  fibrils. This compound was further

studied in our in vitro experiment and was compared with activity of curcumin. The viability of SH-SY5Y cells in the presence of  $\text{A}\beta_{40}$  and  $\text{A}\beta_{42}$  under treatment by propafenone is almost the same extent as curcumin. Through aggregation assay test it was found that the antiamyloidogenic activity of propafenone is slightly better than that of curcumin, with that the IC<sub>50</sub> values for curcumin and propafenone are 2.7 and 1.8  $\mu\text{M}$  with the treatment of  $\text{A}\beta_{40}$ , respectively. This result is in accord with TEM morphology of  $\text{A}\beta_{40}$  in the presence or absence of curcumin and propafenone. Furthermore, the inhibitory ability of free radical production for propafenone is also slightly better than that of curcumin. Thus, both theoretical and experimental results indicate that propafenone is a potential inhibitor for preventing  $\text{A}\beta$  aggregation and inducing cytotoxicity. The binding mechanism of these ligands to  $\text{A}\beta_{40}$  was studied in detail.

## RESULTS AND DISCUSSION

**Choice for Drug Target.** Recent experimental evidence suggested that soluble  $\text{A}\beta$  oligomers are more toxic than mature fibrils<sup>35–38</sup> implying that oligomers should be an appropriate target for designing potential drugs for AD. Using the replica exchange MD method the binding affinity of some ligands to  $\text{A}\beta_{17-42}$  trimer and  $\text{A}\beta_{1-42}$  dimer was probed.<sup>39–41</sup> A similar

**Table 1.** Binding Energy Estimated Using the Docking ( $\Delta E_{\text{bind}}$ ) and FEP ( $\Delta G_{\text{FEP}}$ ) Methods<sup>a</sup>

	$\Delta E_{\text{bind}}$	$\Delta G_{\text{FEP}}^{\text{vdW}}$	$\Delta G_{\text{FEP}}^{\text{elec}}$	$\Delta G_{\text{FEP}}$	$\Delta G_{\text{exp}}$
eterilate	-7.9	-19.90	2.57	$-17.34 \pm 2.37$	
itopride	-7.8	-21.85	-10.01	$-31.85 \pm 6.86$	
propafenone	-8.2	-22.69	-14.44	$-37.13 \pm 5.18$	
FSC	-8.6	-32.75	5.91	$-26.84 \pm 3.19$	-13.95
curcumin	-8.8	-25.14	3.30	$-21.85 \pm 4.26$	-13.33

<sup>a</sup>The experimental binding free energy was calculated from formula  $\Delta G_{\text{exp}} = RT \ln K_i$ , where gas constant  $R = 1.987 \times 10^{-3}$  kcal K<sup>-1</sup> mol<sup>-1</sup>,  $T = 300$  K, and inhibition constant  $K_i$  is measured in moles. Energy is measured in kilocalories per mole. The results obtained for  $\Delta G_{\text{FEP}}$  were averaged over four independent MD trajectories.

study was conducted for oligomers of the human islet amyloid polypeptide segment 22–27.<sup>42</sup>

Structures of full-length A $\beta$  oligomers have not been experimentally resolved, and it remains unclear if they are disordered or highly ordered like protofibrils. In this situation available protofibril/fibril structures of 5A $\beta$ <sub>17–42</sub> (PDB ID: 2BEG<sup>43</sup>), 2-fold symmetry 12A $\beta$ <sub>9–40</sub> (PDB ID: 2LMN and 2LMO<sup>44</sup>), 3-fold symmetry (PDB ID: 2LMP<sup>45</sup>), and the patient-derived fibril (PDB ID: 2M4J<sup>46</sup>), which has a 3-fold symmetry, have been used as target for AD drug design.<sup>11,12,47–50</sup> Our choice of 12A $\beta$ <sub>9–40</sub> structure as a drug target is not only because we follow this strategy but also because in some cases protofibril models provided a reasonable agreement between theoretically estimated ligand binding free energies and experimental data on inhibition constant.<sup>12,48,49</sup> A limited docking simulation for the patient-derived fibril has been also performed to understand diversity of binding modes. This model will be referred to as 9A $\beta$ 1–40 because it has nine full length chains.

#### Selection of Top-Hits from Orally Available Drugs.

The main cause of AD pathogenesis is the formation of toxic A $\beta$  aggregates in the brain of AD patients.<sup>51,52</sup> Preventing or reducing the aggregation and toxicity induced by A $\beta$  has been the primary goal of a number of therapeutic strategies under development or in clinical trials.<sup>53–55</sup> Therefore, in the present study, we screened FDA approved potential drugs with structural similarity to curcumin and studied their antiamyloidogenic activities using both in silico and in vitro approaches.

A Schrodinger package Qikprop,<sup>29</sup> involving the chemical similarity searching functions,<sup>56</sup> was used to search orally available drugs which have more than 80% of chemical and structural similarity with curcumin. Four drugs eterilate, itopride, propafenone, and nilvadipine has been found. Because nilvadipine is currently in phase 3 of clinical trials for AD,<sup>22</sup> only eterilate, itopride, and propafenone (Figure 1B) were conducted for the further study as potential blockers of A $\beta$  aggregation using both theoretical and experimental tools. Similar to curcumin, all of them contain two aromatic rings. For comparison, compound FSC was also studied.

**Binding of Ligands to 12A $\beta$ <sub>9–40</sub>.** Sharing more than 80% of chemical and structural similarities with curcumin (Figure 1C), the binding properties of candidates to A $\beta$  fibrils are expected to be similar to each other. This might be the reason for their close binding positions to curcumin, except a small deviation observed for FSC (Figure 1A and B). The docking binding energy  $\Delta E_{\text{dock}}$  varied little from ligand to ligand (in Table 1) suggesting that curcumin is the best one but this is not certain as the docking energies usually have low correlation with experiments.<sup>14,32</sup> However, binding positions found in the best docking mode are good enough to be used as initial conformations for MD simulations.<sup>11,14,32</sup>

**Molecular Dynamics Simulation.** For each solvated complex, we performed four independent trajectories of MD simulations with the same starting structure but the initial velocity momentum was chosen at random. After three steps of energy minimizations and 100 ps of NVT simulation, 25 ns NPT simulation was performed to search equilibrium structures of solvated receptor–ligand complexes. As follows from the time dependence of the root-mean-square displacement (RMSD), all solvated systems reached equilibrium approximately after 15 ns when RMSD got saturation (Figure 2).

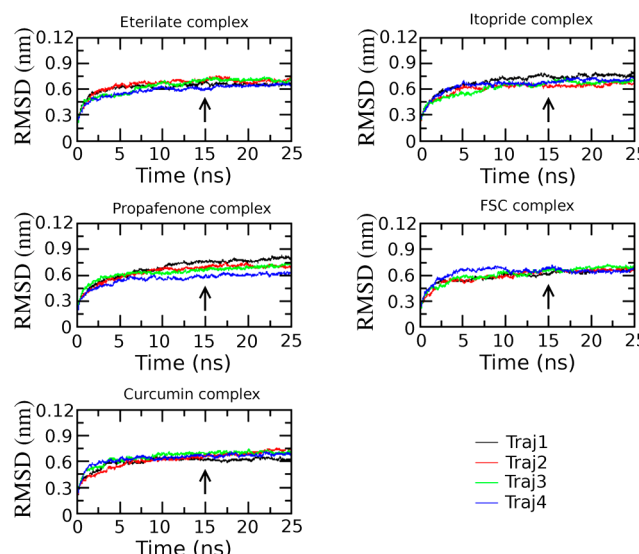


**Figure 2.** Time dependence of RMSD during four NPT MD trajectories of five solvated complexes. RMSD was calculated using coordinates of C $\alpha$  atoms of the peptides. All systems reached equilibrium after about 15 ns denoted by arrow. The last snapshots of these runs were used as initial conformations for subsequent 1 ns MD simulations for free energy calculation by the FEP method.

Conformations, in which a ligand changes its binding position, were not found. This is also evident from Movie S1 in the Supporting Information (SI), where propafenone stays inside fibril during the whole run. RMSD fluctuates around the equilibrium after 25 ns implying that the 25 ns runs are sufficient to fully reach equilibrium. Moreover, the ligand has a minor impact on the stability of fibril leaving RMSD almost the same as in the absence of ligand (Figure 2).

The last snapshot from 25 ns of NPT simulations were used to start new 1 ns MD runs for estimation of  $\Delta G_{\text{bind}}$  using the FEP method. Figures S1 and S2 in the SI show such snapshots for curcumin and propafenone, respectively. The desolvation free energy of ligands in solvent was computed employing the same protocol as for the solvated complex. After energy

minimization of solvated ligands, 100 ps *NVT* MD runs were carried out and then the 2 ns *NPT* simulations were followed. The ligand in solvent remained very stable during *NPT* runs.

**Hydrogen Bonds and Nonbonded Contacts between Ligands and 12A $\beta_{9-40}$ .** Figure S3 shows the number of hydrogen bonds ( $N_{HB}$ ) and nonbonded contacts ( $N_{NB}$ ) between five ligands and fibril as a function of time during 25 ns *NPT* MD runs. Initially, one has  $N_{HB} = 1.13, 1.25, 2, 0.5$ , and 2.75 for eterilate, itopride, propafenone, FSC, and curcumin, respectively. The noninteger value of  $N_{HB}$  comes from averaging over four snapshots. After 15 ns, the number of HBs and nonbonded contacts in all systems fluctuates around its equilibrium value. Averaging over snapshots collected in equilibrium of 4 MD trajectories we obtained  $N_{HB} \approx 2.2, 2.5, 0.4, 1.3$ , and 2.2 for eterilate, itopride, propafenone, FSC, and curcumin, respectively. One can show that  $N_{HB}$  does not correlate with the binding free energies (Table 1), suggesting that the number of hydrogen bonds alone is not sufficient to control ligand binding to A $\beta$  fibril.

In equilibrium the mean value of nonbonded contacts  $N_{NB} \approx 4.4, 5.2, 3.7, 4.4$ , and 4.2 for eterilate, itopride, propafenone, FSC, and curcumin, respectively. As in the case of HBs, there is no correlation between this number and the binding free energy implying that one has to directly compute the interaction energy instead of the bond number.

**Absolute Binding Free Energy.** As mentioned in the Methods section, the 33 independent 1 ns MD simulations were carried for the solvated complexes and ligands with different coupling parameter  $\lambda$ . The free energy was computed every 50 ps. It converged after 250 ps for solvated fibril complexed all ligands (Figure 3). The annihilation free energy

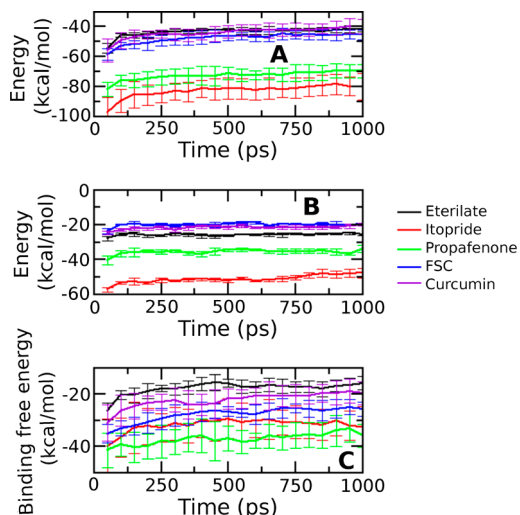


**Figure 3.** Time dependence of binding free energy of five complexes (C). It is defined as a difference between the desolvation free energy of ligand from solvated complexes (A) and desolvation free energy of ligand from solvated ligand (B). The free energy was calculated every 50 ps.

of ligands from both solvated complex and solvated ligand systems fluctuated a little bit because the value of coupling parameter  $\lambda$  changed from 1 to 0. The difference between the annihilation free energies of ligand from solvated ligand and from solvated complex is the absolute binding free energies.<sup>57</sup> Skipping the first 250 ps and averaging over four independence trajectories, we obtained the absolute binding free energy of

ligands to 12A $\beta_{9-40}$  (Table 1). Because the FEP method is one of the most accurate methods, the calculated binding free energies can be used to predict inhibitory activity of candidate compounds. From the top hits, only eterilate has weaker binding affinity in comparison with curcumin. Thus, itopride, FSC, and propafenone are presumably prominent inhibitors for A $\beta$  aggregation. We will further verify the activity of propafenone *in vitro* experiment because it has the highest binding affinity to A $\beta$  with the lowest  $\Delta G_{bind} = -37.13 \pm 5.18$  kcal/mol.

With the equation  $\Delta G_{bind} = RT\ln K_i$ , where gas constant  $R = 1.987 \times 10^{-3}$  kcal K $^{-1}$  mol $^{-1}$ ,  $T = 300$  K, and inhibition constant  $K_i$  is measured in moles, a binding constant of 1 nM corresponds to  $\Delta G_{bind} \approx -12.8$  kcal/mol. A change in  $K_i$  of 1 order of magnitude results in a change in the binding free energy of 1.4 kcal/mol. Therefore, the calculated values of  $\Delta G_{bind}$  (Table 1) imply that  $K_i$  of propafenone could be much less than 1 pM. They are also too far away from the experimentally measured  $K_i$  for FSC and curcumin. The reason behind the discrepancy between theory and experiment is that it is very hard to match the calculated absolute binding free energy with experiments as it depends not only on force fields<sup>58</sup> but also on theoretical methods.<sup>59</sup> However, theoretically estimated binding free energies are presumably useful for ranking binding affinities.<sup>59</sup> This is also evident from our results that, in agreement with experiments, within the error bars FSC and curcumin have the same binding free energy (Table 1). Therefore, our theoretical results on  $\Delta G_{bind}$  are useful for prediction of binding affinity ranking rather than for a direct comparison with experimentally measured inhibition constants.

**Important Role of vdW Interaction on Propafenone Binding to A $\beta$  Fibril and Large Impact of Electrostatics Interaction.** The contribution of vdW and electrostatics interactions to  $\Delta G_{bind}$  is shown in Table 1. In all cases, in agreement with the previous study,<sup>14</sup> the vdW interaction is a major contributor. The strongest vdW interaction was seen for FSC but its binding affinity is lowered by the repulsive electrostatic interaction. The vdW term of propafenone is nearly equal to itopride and curcumin, but its electrostatics interaction, which contributes  $\approx 38.9\%$  of the total  $G_{FEP}$ , is larger than not only itopride and curcumin but also other compounds. This explains the domination of propafenone over other ligands in binding affinity to 12A $\beta_{9-40}$ .

In order to shed more light on the nature of propafenone binding mechanism we compare contributions of its individual atoms with those of curcumin (Figure S4). Atomic charges and masses of these compounds are listed in Tables S5 and S7. Because studying individual contributions by the FEP method is difficult, the molecular mechanic-Poisson–Boltzmann surface area (MM-PBSA) method (see Methods) was adopted to deal with this problem. Here the electrostatic, vdW, polar, and nonpolar terms of the binding free energy (eq 1) are computed separately.

For both curcumin and propafenone, carbon atoms make the major contribution to the vdW interaction (Figures S5 and S6) regardless of their position on or off rings. Because two ligands have the same number of carbon atoms the vdW interaction energies are nearly the same as shown by the FEP calculation (Table 1) or by the simple estimation of the interaction energy by MM-PBSA (Figure S5 and S6). The latter method gives  $\Delta E_{vdW} = -60.67$  and  $-61.13$  kcal/mol (Table S1 in the SI), for curcumin and propafenone, respectively. Note that this result is different from the FEP result shown in Table 1 because in the

FEP method the vdW contribution was estimated as the difference between the desolvation energies from solvated complex and ligand. The contribution from two rings is 49.84 and 53.98% for curcumin and propafenone, respectively.

The main difference between curcumin and propafenone comes from the electrostatic interaction with minor contribution from rings. For curcumin atoms, O<sub>3</sub>, H<sub>3</sub>, O<sub>1</sub>, C<sub>26</sub>, O<sub>5</sub>, C<sub>20</sub>, O<sub>6</sub>, C<sub>21</sub>, O<sub>2</sub>, C<sub>27</sub>, O<sub>4</sub>, and H<sub>4</sub> contribute substantially (Figure S7) because they have large charges (Table S7) forming quasi-dipoles O<sub>3</sub>–H<sub>3</sub>, O<sub>1</sub>–C<sub>26</sub>, O<sub>5</sub>–C<sub>20</sub>, O<sub>6</sub>–C<sub>21</sub>, O<sub>2</sub>–C<sub>27</sub>, and O<sub>4</sub>–H<sub>4</sub> (they are called quasi-dipoles as their charges are not fully compensated). Among them the contribution of O<sub>3</sub>–H<sub>3</sub> pair is the most prominent. The total electrostatic interaction energy between curcumin and fibril is  $\Delta E_{\text{elec}} = -28.16 \text{ kcal/mol}$ .

As seen from Figure S8, quasi-dipoles H<sub>26</sub>–O<sub>2</sub>, O<sub>1</sub>–C<sub>7</sub>, and O<sub>3</sub>–C<sub>14</sub>, and particularly the block consisting of C<sub>8</sub>, N<sub>4</sub>, H<sub>41</sub>, H<sub>42</sub>, and C<sub>6</sub> mainly control the electrostatic interaction of propafenone. These atoms possess the absolute charge exceeding 0.31e (Table S5). The contribution of block [C<sub>8</sub>, N<sub>4</sub>, H<sub>41</sub>, H<sub>42</sub>, C<sub>6</sub>] is 84.36% of the total  $\Delta E_{\text{elec}} = -248.97 \text{ kcal/mol}$ . Because the contribution of this fragment is crucial we speculate that its presence in other ligands enhances the binding affinity to A $\beta$  fibril. This observation may be valuable for designing potential drugs for AD.

Using the MM-PBSA method we obtained  $\Delta G_{\text{sur}} = -6.73$  and  $-6.53 \text{ kcal/mol}$  for curcumin and propafenone, respectively. Thus, the nonpolar contributions or hydrophobic interactions are nearly the same for two ligands presumably because solvent accessible surface areas (SASAs) do not differ much due to high ligand structural similarity.

Contrary to the nonpolar interaction, the polar term  $\Delta G_{\text{PB}}$  is drastically different for curcumin ( $\Delta G_{\text{PB}} = 46.20 \text{ kcal/mol}$ ) and propafenone ( $\Delta G_{\text{PB}} = 256.97 \text{ kcal/mol}$ ) complexes due to the stronger polarization effect resulting from higher atomic charges of the former compared to the latter (Table S5 and S7). The entropy term of curcumin is larger than propafenone (Table S1 in the SI). In agreement with the FEP results, MM-PBSA method also revealed that propafenone binds to fibril stronger than curcumin. Interestingly, within the error bars two methods provided the same binding free energy for two compounds.

**Ligand Binding Site in 2-fold Symmetry Fibril 12A $\beta$ <sub>9–40</sub>.** As evident from Figure 1 and Movie 1, ligands locate near the turn in the lower layer. A more detailed information about their position can be obtained monitoring the population of the nonbonded contacts between centers of mass of ligand and fibril residues in equilibrium. Using snapshots collected in the last 10 ns in the four MD trajectories of 25 ns we obtained the results shown in Figures S9 and S10 in the SI. Considering only those contacts that have population exceeding 20%, one can see that eterilate predominantly forms contact with hydrophobic residues Ala21D, Ala21E, Ala21F, Ala30F, Ile31F, Ile32E and Ile32F, and polar residue Lys28F (Table S2 in the SI). All ligands prefer to position next to alanine (Ala) and isoleucine (Ile) from different chains. Except curcumin, the high population with charged residue Lys28 was observed. Residue Asp23, which may form salt bridge with Lys28, prefers to stay away from ligand in all cases (Figures S9 and S10). Only curcumin and propafenone very often form contact with polar but neutral asparagine at position 27 of chain D. Taken together, ligands mainly interact with hydrophobic residues in the turn region of fibril.

**Ligand-Induced  $\beta$ -Content Change.** Prior works have provided evidence that the higher binding affinity is the stronger is A $\beta$  structure stability and aggregation inhibition.<sup>14,60</sup> Using snapshots collected in equilibrium for solvated complexes, the  $\beta$ -content of 12A $\beta$ <sub>9–40</sub> fibril were analyzed using DSSP tool<sup>61,62</sup> (Figure S11). In the presence of propafenone, the  $\beta$ -content decreased to the largest extent that is expected to be in line with the hypothesis that the tight ligand binding would strongly degrade A $\beta$ <sub>9–40</sub> fibrils. In equilibrium the fibril with curcumin has  $\beta$ -content of 57.8% which is higher than 52.6% of the propafenone complex. Thus, propafenone is slightly better than curcumin in A $\beta$  fibril degradation.

For the five studied ligands we have found a good correlation (correlation level  $R = 0.93$ ) between the binding free energies estimated by the FEP method and the  $\beta$ -content of A $\beta$  (Figure S12 in the SI). A similar analysis was not carried out for the correlation with experiments because the experimental binding free energy was known only for two compounds FSC and curcumin (Table 1).

**Ligand Binding Site in Patient-Derived Fibril 9A $\beta$ <sub>1–40</sub>.** Contrary to the 12A $\beta$ <sub>9–40</sub> case, in the best docking mode five ligands do not bind to the same position in the 3-fold symmetry structure 9A $\beta$ <sub>1–40</sub> (Figure S13 in the SI, upper panel). Eterilate and curcumin have the same location, while itopride, FSC, and propafenone bind to different places. Propafenone is bound to the N-terminals of three chains B, E, and H of 9A $\beta$ <sub>1–40</sub> (Figure S13 in the SI, lower panel), whereas it interacts with the turn region of the 2-fold symmetry target 12A $\beta$ <sub>9–40</sub> (Figure 1A). Among five ligands only FSC has the binding site near the turn region similar to the binding pose of propafenone in 12A $\beta$ <sub>9–40</sub> fibril (Figures 1A and S13). However, their binding sites are not identical as two targets share with FSC only six common contacts with Phe19, Phe20, Asp23, Lys28, Ile31, and Leu34 from different chains (Figure S14). Note that in the best docking mode FSC has 32 and 10 contacts with 12A $\beta$ <sub>9–40</sub> and 9A $\beta$ <sub>1–40</sub>, respectively.

Except FSC, the ligands are positioned outside fibril leading to the lower binding affinity compared to 12A $\beta$ <sub>9–40</sub> target. The binding energy  $\Delta E_{\text{bind}}$  for five ligands falls in the range of [-7.8, -8.8] and [-5.0, -6.0 kcal/mol] for the 12A $\beta$ <sub>9–40</sub> and 9A $\beta$ <sub>1–40</sub> protofibrils, respectively, suggesting that they bind to the former target stronger than to the second one. However, this result was obtained by the docking method which is not accurate enough for predicting binding affinities. Although more sophisticated are required to estimate the binding free energy, the binding modes of ligands including propafenone strongly depend on the structure of target.

**Cell Viability in the Presence and Absence of Curcumin or Propafenone.** As shown in the in silico studies, propafenone is better than curcumin on the binding affinity and antiamyloidogenic activity. Therefore, we further verified if these results are consistent with in vitro experiments.

First, we examined the protective effects of curcumin and propafenone on the A $\beta$ <sub>40</sub> induced toxicity using MTT cell viability assay. Figure 4 shows the related cell viability with the treatment of different concentrations of curcumin and propafenone incubated for 72 h. The cell survival rate showed a dose-dependent mode for both curcumin and propafenone. When the concentration above 1  $\mu\text{M}$ , both curcumin and propafenone showed a significant protection of SH-SY5Y cells against A $\beta$ <sub>40</sub> induced toxicity. Cell survival rate was increased from 55%, with 10  $\mu\text{M}$  A $\beta$ <sub>40</sub> only, to more than 90%, with the

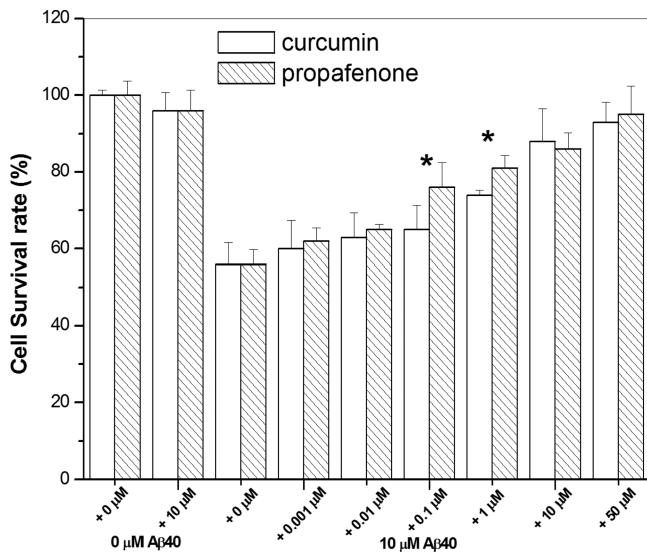


**Figure 4.** Cell viability with or without treatment of curcumin or propafenone determined by the MTT assay. Survival percentages of SH-SY5Y cells incubated with 10  $\mu\text{M}$   $\text{A}\beta_{40}$  for 72 h. Wells containing SH-SY5Y cells without  $\text{A}\beta$  peptides were used as a control group. The difference of cell survival rate between the treatment of curcumin and propafenone at concentration of 0.1 and 1  $\mu\text{M}$  was significant. (\*:  $P \leq 0.05$ ).

treatment of 50  $\mu\text{M}$  curcumin or propafenone. However, the cell survival rate shows no significant difference between the treatment of curcumin and propafenone when the concentration is  $\geq 10$  or  $\leq 0.01 \mu\text{M}$ . At the concentration between 0.1 and 1  $\mu\text{M}$ , the cell survival rate with the treatment of propafenone is slightly better than that with the treatment of curcumin.

We further tested the protection ability of curcumin and propafenone against  $\text{A}\beta_{42}$  induced cytotoxicity. Figure S15 of the SI showed the cell survive rate with the treatment of various concentrations of curcumin and propafenone. Similarly, the protective ability of propafenone was also better than that of curcumin. The effect is even more significant with respect to the cell survive rate at the concentration  $\geq 0.1 \mu\text{M}$ ; propafenone showed better resistance to  $\text{A}\beta_{42}$  induced cytotoxicity than curcumin.

**Aggregation Assay of the  $\text{A}\beta$  Peptide in the Presence and Absence of Curcumin or Propafenone.** The cytotoxicity induced by  $\text{A}\beta$  is raised from the property of  $\text{A}\beta$  self-aggregation. As shown in the prior result, both curcumin and propafenone could protect the cell against  $\text{A}\beta$  induced toxicity on a dose-dependent manner. Therefore, we then investigated the inhibitory ability of curcumin and propfenone on the aggregation kinetics for  $\text{A}\beta_{40}$  and  $\text{A}\beta_{42}$ .

Figures 5A and B and S16A and B show the aggregation process for  $\text{A}\beta_{40}$  and  $\text{A}\beta_{42}$  in the presence of curcumin and propafenone using the Th-T binding assay, respectively. It can be seen that the inhibition of  $\text{A}\beta_{40}$  and  $\text{A}\beta_{42}$  aggregation by

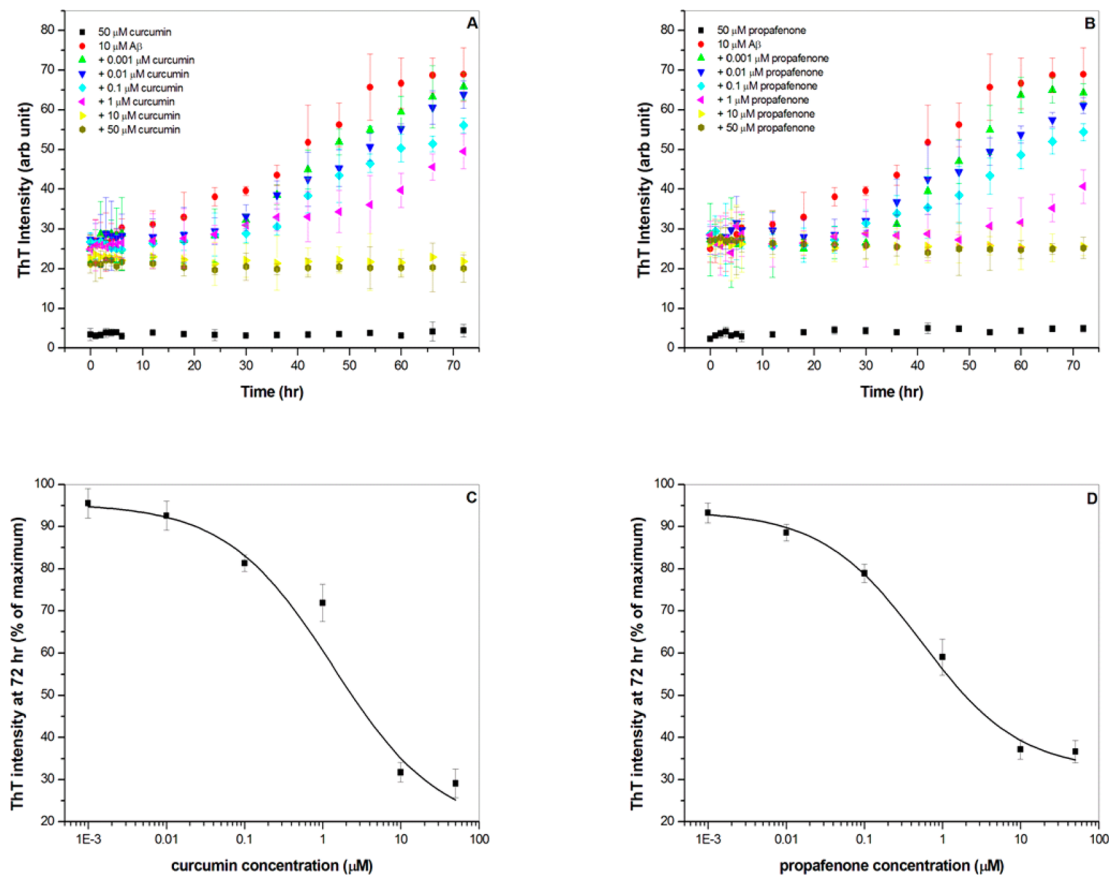


**Figure 5.** Kinetics of the aggregation process of  $\text{A}\beta_{40}$  with or without treatment of curcumin or propafenone. (A) Aggregation process of  $\text{A}\beta_{40}$  with the treatment of various concentrations of curcumin. (B) Aggregation process of  $\text{A}\beta_{40}$  with the treatment of various concentrations of propafenone. The estimation of IC<sub>50</sub> value for (C) curcumin and (D) propafenone at 72 h. The aggregation assay was performed with 10  $\mu\text{M}$   $\text{A}\beta$  peptides.

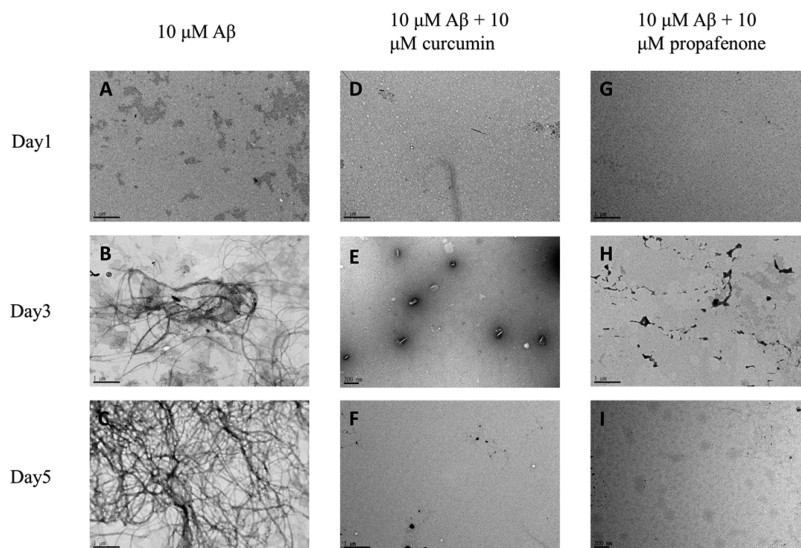


**Figure 6.** TEM images of  $\text{A}\beta_{40}$  morphologies with or without treatment of curcumin or propafenone. Fibrils formed from  $10 \mu\text{M} \text{ A}\beta$  peptides without or with treatment of curcumin or propafenone in phosphate buffer, pH 7.0,  $37^\circ\text{C}$  at days 1, 3, and 5, (A–C) with  $10 \mu\text{M} \text{ A}\beta_{40}$  only, (D–F) with treatment of  $10 \mu\text{M}$  curcumin, and (G–I) with treatment of  $10 \mu\text{M}$  propafenone. All TEM images are  $200\,000\times$  magnification. The scale bar indicates 200 nm.

curcumin and propafenone was also concentration-dependent. In consistent with the result of cell viability assay, both curcumin and propafenone could significantly inhibit either  $\text{A}\beta_{40}$  or  $\text{A}\beta_{42}$  aggregation at concentration  $\geq 10 \mu\text{M}$ . At concentration  $\leq 0.1 \mu\text{M}$ , both curcumin and propafenone could not inhibit the aggregation of  $\text{A}\beta_{40}$  peptides. At concentration between 10 and  $0.1 \mu\text{M}$ , the antiamyloidogenic activity of propafenone is similar to that of curcumin.

IC<sub>50</sub> values for curcumin and propafenone were estimated from the plot of Th-T intensity vs concentration of curcumin and propafenone as shown in Figure 5C and D for  $\text{A}\beta_{40}$  and Figure S16A and B for  $\text{A}\beta_{42}$ , respectively. The estimated IC<sub>50</sub> values in the case of  $\text{A}\beta_{40}$  are  $2.7 \pm 0.7$  and  $1.8 \pm 0.2 \mu\text{M}$  for curcumin and propafenone, respectively, while the IC<sub>50</sub> values in the case of  $\text{A}\beta_{42}$  are much higher,  $6.9 \pm 0.9$  and  $3.9 \pm 0.8 \mu\text{M}$  for curcumin and propafenone, respectively. Our obtained IC<sub>50</sub> is very close the reported values which IC<sub>50</sub> values for curcumin reported in literature were ranged  $0.8\text{--}10 \mu\text{M}$ .<sup>13,63</sup> It is noted that curcumin has a strong absorption at 440 nm which this might make underestimation of IC<sub>50</sub> for curcumin.<sup>64</sup> However, from our present results, the IC<sub>50</sub> values of propafenone are moderately lower than those of curcumin. This is generally consistent with the in silico studies which shows that propafenone has stronger binding affinity and antiamyloidogenic activity than curcumin. Taken together, both in silico and in vitro studies support that the inhibitory ability of propafenone is slightly better than or similar to that of curcumin. It should be noted that IC<sub>50</sub> presented here reflects capability of propafenone and curcumin to inhibit lag and growth phases, but not equilibrium phase because it was obtained using nonequilibrium data (Figure 5).

**Transmission Electron Microscopic (TEM) Morphology of  $\text{A}\beta$  Aggregates.** As results demonstrated in the aggregation assay, both curcumin and propafenone can significantly inhibit the aggregation of  $\text{A}\beta_{40}$  at the concentration higher than  $10 \mu\text{M}$ . Therefore, we applied TEM to observe the morphology of  $\text{A}\beta_{40}$  in the absence and presence of curcumin and propafenone. The TEM morphologies of  $\text{A}\beta_{40}$  at various days are shown in Figure 6A–I. As shown in Figure 6A, B, and

C, in the absence of curcumin ( $1 \mu\text{M}$ ) and propafenone ( $1 \mu\text{M}$ ), the morphology of  $\text{A}\beta_{40}$  gradually aggregated into a fibril at days 3 and 5, while as shown in Figure 6D–F and G–I for the existence of  $10 \mu\text{M}$  curcumin and propafenone respectively, no fibrillary morphologies could be observed through the whole incubation time at  $37^\circ\text{C}$ , further indicating that the aggregation of  $\text{A}\beta_{40}$  was effectively inhibited by both curcumin and propafenone.

**Free Radical Assay with or without the Treatment of Curcumin or Propafenone.** The production of free radical by  $\text{A}\beta$  peptide has been proposed as one of the cause to cell death.<sup>56,57,65</sup> Therefore, we examined the inhibition of  $\text{A}\beta_{40}$  induced free radical generation for curcumin and propafenone using the DCF assay. Figure 7A and B show the DCF fluorescence intensity of  $\text{A}\beta_{40}$  alone and in the presence of various concentrations of curcumin and propafenone incubated for 0, 12, 24, 36, and 48 h, respectively. In both Figure 7A and B, the DCF fluorescence intensity of  $\text{A}\beta_{40}$  in the absence of curcumin or propafenone was generally increased with an increase of incubation time. For the concentration lower than  $1 \mu\text{M}$ , the inhibition of free radical production was not significant for both curcumin and propafenone, whereas the production of free radical was significantly inhibited when the concentration  $\geq 10 \mu\text{M}$  for both curcumin and propafenone. At the concentration  $\geq 10 \mu\text{M}$ , the inhibitory effect shows no obvious difference between curcumin and propafenone.

At concentrations between  $0.1$  and  $10 \mu\text{M}$ , propafenone showed a better inhibitory ability than curcumin. In comparison with the DCF intensity of  $\text{A}\beta_{40}$  alone, the DCF fluorescence intensity was decreased by 25% and 45% in the presence of  $1 \mu\text{M}$  curcumin and propafenone, respectively, when incubated for 36 h. The DCF fluorescence intensity was decreased by 40% and 55% in the presence of  $5 \mu\text{M}$  curcumin and propafenone, at 36 h, respectively. The results obtained from free radical assays for curcumin and propafenone are in agreement with the cell viability and aggregation assays. Propafenone is better than curcumin on antiamyloidogenic activity, reduction of free radical production and cytotoxicity induced by  $\text{A}\beta$ . Taken together, our results suggest that the protection of SH-SY5Y

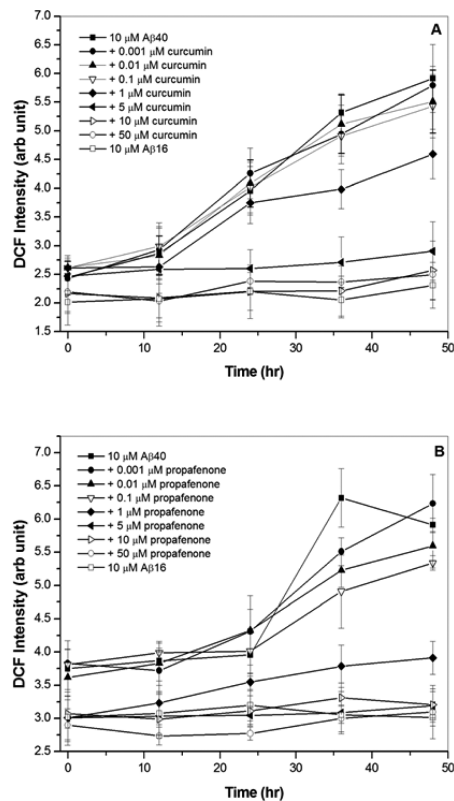


**Figure 7.** DCF free radical assay in the presence and absence of curcumin or propafenone. (A) Free radical generation for either 10  $\mu\text{M}$  of  $\text{A}\beta_{40}$  alone or 10  $\mu\text{M}$  of  $\text{A}\beta_{40}$  in the presence of 0.001, 0.01, 0.1, 1, 5, 10, and 50  $\mu\text{M}$  curcumin at 0, 12, 24, 36, and 48 h. (B) Free radical generation for either 10  $\mu\text{M}$  of  $\text{A}\beta_{40}$  alone or 10  $\mu\text{M}$  of  $\text{A}\beta_{40}$  in the presence of 0.001, 0.01, 0.1, 1, 5, 10, and 50  $\mu\text{M}$  propafenone at 0, 12, 24, 36, and 48 h.

cells against  $\text{A}\beta$  toxicity may be through the reduction of  $\text{A}\beta$  aggregation and subsequent induced free radical damage for both propafenone and curcumin.

In conclusion, both theoretical and experimental studies indicated that similar to curcumin, propafenone could effectively protect cell against  $\text{A}\beta$  induced cytotoxicity through the inhibition of  $\text{A}\beta$  aggregation and reduction of the free radical caused damage. Furthermore, compared to the protective efficacy of curcumin, propafenone proves to be more effective on the prevention of  $\text{A}\beta$ -induced aggregation, free radical production, and cytotoxicity. This makes propafenone an attractive candidate for further clinical trial for the treatment of AD. Further new design of antiamyloidogenic compounds based on the structure feature of propafenone will be promising for the future development of effective drugs used on the treatment of AD. We have found that the existence of nitrogen and related carbon and hydrogen atoms in propafenone substantially increases its binding affinity compared to curcumin via enhanced electrostatics interaction. This observation may be valuable for drug design for Alzheimer's disease but much more work is required to cement it.

## METHODS

**Screening Top Hits by Chemical and Structural Similarity with Curcumin.** The similarity between two compounds was estimated through association and distance

coefficients. The Tanimoto's association coefficient<sup>66,67</sup> was characterized for binary data:

$$S_{A,B} = \frac{\sum_{i=1}^n p_{iA} p_{iB}}{\sum_{i=1}^n p_{iA}^2 + \sum_{i=1}^n p_{iB}^2 - \sum_{i=1}^n p_{iA} p_{iB}}$$

where  $S_{A,B}$  is the similarity score between molecules A and B and  $p_{iA}$  and  $p_{iB}$  are the values describing the properties for molecules A and B such as hydrophobic and hydrophilic solvent accessible surface area, HB donor, HB acceptor, polarizability, and aqueous solubility. The distance coefficients  $D_{A,B}$  are the score of the difference between two molecules A and B:<sup>68</sup>

$$D_{A,B} = [\sum_{i=1}^n m_i (p_{iA} - p_{iB})^2]^{1/2}$$

where  $m_i$  is the corresponding mass. To screen out potential candidates for AD we used QikProp implemented in Schrodinger package.<sup>28</sup> Compounds that share  $\geq 80\%$  similarity with curcumin were selected.

**Structure Model of Fibril and Ligands.** Chemical structures of eterilate (44258), itopride (3792), propafenone (4932), FSC (16087306), and curcumin (969516) are downloaded from Pubchem database<sup>68</sup> (Figure 1B). The solid state NMR structures of fibril 12 $\text{A}\beta_{9-40}$  (PDB ID: 2LMN<sup>44</sup>) and 9 $\text{A}\beta_{1-40}$  (PDB ID: 2MJ<sup>46</sup>) retrieved from the protein databank were used for simulation.

**Docking Method.** Starting structures of 12 $\text{A}\beta_{9-40}$ -ligand complexes were generated by using Autodock Tools 1.5.6.<sup>69</sup> Autodock Vina version 1.1<sup>70</sup> was employed to dock ligands to 2-fold 12 $\text{A}\beta_{9-40}$  fibril. This docking package uses the Broyden–Fletcher–Goldfarb–Shanno (BFGS) method<sup>71</sup> for local optimization. Atom types were described by the CHARMM force field.<sup>72,73</sup> The center of grids was placed at the center of receptor and grid dimensions were chosen large enough ( $80 \times 60 \times 40 \text{ \AA}^3$  for 12 $\text{A}\beta_{9-40}$  and  $94 \times 98 \times 40$  for 9 $\text{A}\beta_{1-40}$ ) to cover the whole target. In the docking simulation  $\text{A}\beta$  peptides were kept rigid, while the ligand was allowed to freely flex all of its torsion degrees of freedom. The maximum difference between energies of the best and the worse binding modes was chosen as large as 7 kcal/mol with 20 binding modes generated starting from random configurations of ligand. The exhaustiveness was set to 600 which is good enough to produce reliable results.

**Molecular Dynamics Simulation.** The lowest binding energy configurations, obtained by the docking method, were used as the starting configurations for MD runs. The initial structures of all complexes are shown in Figure 1A. The GROMACS 4.5.5 package<sup>74</sup> was employed for MD simulation. The receptor and water molecules were represented using the Gromos96 43a1 force field<sup>75,76</sup> and SPC water model,<sup>77</sup> respectively. The geometric parameters of ligands were generated by the PRODRG2 beta server,<sup>78</sup> while the parameter of charges and charge groups were provided using restrained electrostatic potential (RESP) method<sup>79</sup> at the Hartree–Fock (HF)/6-31G(d) level in the gas phase. The type, mass and charge of each atom of the studied ligands are given in Tables S3–S7 in the SI.

The MD simulation parameters (relaxation time 0.1 ps, pressure 1.0 atm, and temperature 300 K) were the same as in our previous work.<sup>32</sup> Hydrogen bonds were constrained by LINCS<sup>80</sup> with order 8. The cutoff of neighbor nonbonded pair

was 1.0 nm and updated every 10 fs. The electrostatics interaction was computed by the fast smooth particle mesh Ewald electrostatics (PME) method<sup>81</sup> with a cutoff 0.9 nm for the Lennard-Jones interaction. The complexes and ligands were put into the dodecahedron boxes which contained approximate 21,000 and 1,000 water molecules, respectively. The periodic boundary conditions were applied to reduce size effects. The solvated systems were neutralized adding counterions Na<sup>+</sup> and Cl<sup>-</sup>.

First the solvated systems were minimized by the steepest descent, conjugate gradient and low-memory BFGS methods.<sup>71</sup> As the maximum force drops below  $2 \times 10^{-6}$  kJ mol<sup>-1</sup> mn<sup>-1</sup> for the solvated complex and  $10^{-6}$  kJ mol<sup>-1</sup> mn<sup>-1</sup> for the solvated ligand, the minimization procedure was stopped. Then, systems were relaxed in the position restrained simulation for 100 ps. NPT simulations of 25 and 2 ns were followed to search equilibrium states of solvated complexes and solvated ligands, respectively. The last snapshots of NPT simulations were used for the binding free energy calculations by the FEP method.

**Free Energy Perturbation Method.** To obtain more accurate binding energy, the FEP method<sup>32,34,82</sup> was employed to compute the binding free energy of ligands to 12A $\beta_{9-40}$ . Details of this method was described elsewhere.<sup>32</sup> Basically, 21 values of  $\lambda$  (coupling parameter) were used to reduce the vdW interaction from full ( $\lambda = 1$ ) to none ( $\lambda = 0$ ). Similarly, 12 values of  $\lambda$  (from 1 to 0) were chosen to decrease the electrostatics interaction using a soft core potential.<sup>33,83</sup> The set of  $\lambda$  were the same in both the solvated complex and ligand systems ( $\lambda = 0.0, 0.1, 0.2, 0.275, 0.375, 0.45, 0.55, 0.65, 0.675, 0.725, 0.75, 0.775, 0.8, 0.825, 0.85, 0.875, 0.9, 0.925, 0.95, 0.975$ , and 1.0 for adjustment of vdW interaction, and  $\lambda = 0.00, 0.10, 0.25, 0.45, 0.55, 0.65, 0.70, 0.75, 0.80, 0.90, 0.95$ , and 1.00 for adjustment of Coulomb interaction). The binding free energy  $\Delta G_{\text{bind}}$  was estimated using BAR method<sup>34</sup>  $\Delta G_{\text{bind}} = G_A - G_B$ . Here,  $G_A$  and  $G_B$  represent the free energy of ligand desolvation from solvated complex and the free energy of ligand from solvated ligand system, respectively. The reported results were averaged over 8 independent MD trajectories for each complex.

**MM-PBSA Method.** Because the FEP does not allow for separating polar and nonpolar components of the electrostatic interaction we will use the MM-PBSA method to study this problem. In the MM-PBSA method the ligand binding free is decomposed into the following terms<sup>84</sup>

$$\Delta G_{\text{bind}} = \Delta E_{\text{elec}} + \Delta E_{\text{vdW}} + \Delta G_{\text{sur}} + \Delta G_{\text{PB}} - T\Delta S \quad (1)$$

Here  $\Delta E_{\text{elec}}$  and  $\Delta E_{\text{vdW}}$  are electrostatic and vdW interaction energies, respectively, while  $\Delta G_{\text{sur}}$  and  $\Delta G_{\text{PB}}$  are nonpolar and polar solvation energies. The conformational entropy of the solute  $S$  was estimated by normal-mode analysis by diagonalizing the mass-weighted Hessian matrix.<sup>85</sup> Snapshots collected in equilibrium and eq 1 were used to compute  $\Delta G_{\text{bind}}$ . The absolute nonpolar solvation term  $G_{\text{sur}}$  was approximated as  $G_{\text{sur}} = \gamma_{\text{SASA}} \text{SASA}$  is estimated by the Shrake-Rupley numerical method<sup>86</sup> integrated in the APBS package<sup>87</sup> in Gromacs and  $\gamma = 0.0072$  kcal mol<sup>-1</sup> Å<sup>-2</sup>.<sup>88</sup> The polar contribution  $G_{\text{PB}}$  was derived from the electrostatic potential between solute and solvent solving the corresponding linear Poisson-Boltzmann equation in a continuum medium. More details are available in our previous work.<sup>58</sup>

**Data Analysis.** The hydrogen bond formation should satisfy the criteria that the distance between donor D and acceptor A is  $\leq 3.5$  Å and the D-H-A angle is  $\geq 135^\circ$ . A

nonbonded contact between the ligand and receptor residue is formed if the distance between their centers of mass is less than 0.65 nm. RMSD of the fibril from the initial configuration was computed using positions of C $\alpha$  atoms of residues. The secondary structures were analyzed using DSSP tool.<sup>54,55</sup> For instance, discretizing dihedral angles  $\varphi$  and  $\psi$  into 20 intervals of  $18^\circ$  each, the  $\beta$ -strand conformations correspond to vertices of the polygon  $(-180^\circ, 180^\circ), (-180^\circ, 126^\circ), (-162^\circ, 126^\circ), (-162^\circ, 108^\circ), (-144^\circ, 108^\circ), (-144^\circ, 90^\circ), (-50^\circ, 90^\circ)$ , and  $(-50^\circ, 180^\circ)$  on the Ramachandran plot. Molecular structures were visualized by PyMol.

**A $\beta_{40}$  Synthesis and Purification.** A $\beta_{40}$  peptides were synthesized in a solid-phase peptide synthesizer (PS3, Protein Technologies, Inc., AZ) using standard FMOC protocols with HMP resin. After cleavage from the resin by stirring with a mixture of trifluoroacetic acid/H<sub>2</sub>O/ethanedithiol thiol anisole/phenol for 3 h, the peptides were then extracted using ether: H<sub>2</sub>O (1:1 v/v) mixture. The synthesized A $\beta_{40}$  peptides were purified using a C18 reverse-phase column with a linear gradient from 0% to 80% acetonitrile. Peptide purity was over 95% as identified by mass spectroscopy. One milligram of A $\beta_{40}$  peptide was dissolved in 1 mL trifluoroethanol and then centrifuged (20 000g) to sediment the insoluble particles. This A $\beta_{40}$  solution was then dried using freeze-dryer and stored at  $-80^\circ\text{C}$  until used.

**Cell Cultures.** Human blastoma SH-SY5Y cells were cultured in minimum essential medium supplemented with 50% (v/v) F-12 nutrient mixture, 10% (v/v) heat-inactivated fetal bovine serum, and 1% (v/v) antibiotics comprised of penicillin and streptomycin. Cells were kept at  $37^\circ\text{C}$  in a humidified atmosphere of 5% CO<sub>2</sub>. SH-SY5Y cells were plated at a density of  $5 \times 10^4$  viable cells per well in 96-well plates for further analyses.

**Cell Viability Assay.** The cell viability was measured using the MTT assay. A 1 mg portion of A $\beta_{40}$  was dissolved in 1000  $\mu\text{L}$  trifluoroethanol, dried under N<sub>2</sub> gas, redissolved in DMSO, and incubated at  $4^\circ\text{C}$  for 12 h to make a 500  $\mu\text{M}$  of peptide stock solution. For the viability assay,  $5 \times 10^4$  cells were incubated in a 96-well microtiter plate containing either 10  $\mu\text{M}$  incubated A $\beta$  peptides only, or 10  $\mu\text{M}$  incubated A $\beta$  peptides with various concentrations of curcumin or propafenone. The reaction was carried out for 72 h at  $37^\circ\text{C}$  in a humidified atmosphere containing 5% CO<sub>2</sub> before cell viability was assayed. A 10  $\mu\text{L}$  portion of MTT were added to each well, and the wells were incubated for another 8 h at room temperature. The optical density was determined at 450 nm, using a microplate reader (FlexStation 3, MD).

**Aggregation Assay.** Thioflavin-T (ThT) was used to monitor the aggregation state of A $\beta_{40}$ . All samples containing a peptide concentration of 10  $\mu\text{M}$  in the absence and presence of various concentrations of curcumin or propafenone and 3  $\mu\text{M}$  ThT were incubated at  $37^\circ\text{C}$ . Samples containing either A $\beta$  peptide only or A $\beta$  with curcumin or propafenone, taken daily from 0 to 72 h, were used to measure the ThT intensity. The Th-T fluorescence intensity was measured using a microplate reader (FlexStation 3, MD) at  $37^\circ\text{C}$  with the excitation and emission wavelengths of 440 and 485 nm, respectively.

**Transmission Electron Microscope Analysis.** A 5  $\mu\text{L}$  portion of the A $\beta$  peptide samples without or with treatment of 10  $\mu\text{M}$  curcumin or propafenone for the aggregation assay at days 1, 3, and 5 were placed onto a carbon-coated 200 mesh copper grid (Pelco, Ca, USA). The grid containing sample was allowed to air-dry and then stained with 1 mL of 2% uranyl

acetate for 30 s. The grid was first wicked dry with tissue paper to remove the excess solution and then allowed to air-dry before TEM analysis. A transmission electron microscope (JEM-2000 EXII, JEOL, Japan) with an accelerating voltage of 100 keV was used to analyze the morphology of  $\text{A}\beta$  peptides.

**Free Radical Assay.** The level of hydroxyl radicals induced by  $\text{A}\beta_{40}$  in cell free conditions was analyzed using the dichlorofluorescein diacetate (DCF-DA) assay.<sup>89</sup> Basically, DCF-DA was first deacetylated with 50% (v/v) 0.05 M NaOH for 30 min and then neutralized to pH 7.5. A final concentration of 200  $\mu\text{M}$  deacetylated DCF was prepared as a stock solution and kept on ice in the dark until further use. The reactions were carried out in a 96-well plate (200  $\mu\text{L}/\text{well}$ ) containing 10  $\mu\text{M}$  of  $\text{A}\beta_{40}$  peptides, 5  $\mu\text{M}$  horseradish peroxidase, and 15  $\mu\text{M}$  deacetylated DCF, in Dulbecco's phosphate-buffered saline, pH 7.5 (Sigma, USA). To determine the inhibitory effects of curcumin and propafenone on inhibition of free radical formation, either curcumin or propafenone with concentrations of 0.001–50  $\mu\text{M}$  were added and incubated at 37 °C. Fluorescence readings were recorded on amicroplate reader (FlexStation 3, MD) with the excitation wavelength of 485 nm and the emission wavelength of 530 nm. The fluorescence intensity of DCF was measured every 12 h and from 0 to 48 h.

## ■ ASSOCIATED CONTENT

### Supporting Information

The Supporting Information is available free of charge on the ACS Publications website at DOI: [10.1021/acs.jcim.6b00029](https://doi.org/10.1021/acs.jcim.6b00029).

Figures S1 and S2: last snapshots obtained in four MD runs of 25 ns for curcumin and propafenone, respectively. Figure S3: time evolution of number of HBs and nonbonded contacts between five ligands and 12 $\text{A}\beta_{9-40}$  peptides. Figure S4: atomic structures of curcumin (35 atoms) and propafenone (37 atoms). Figures S5 and S6: per-atom contributions to the vdW interaction energy between curcumin or propafenone, respectively, and 12 $\text{A}\beta_{9-40}$ . Figures S7 and S8: per-atom contributions to the interaction energy between curcumin or propafenone, respectively, and 12 $\text{A}\beta_{9-40}$ . Figures S9 and S10: populations of nonbonded contacts between fibril and ligand. Figure S11:  $\beta$ -content of 2-fold  $\text{A}\beta_{40}$  peptides in complex with five ligands. Figure S12: correlation between the binding free energy and the  $\beta$ -content. Table S1: binding free energy (kcal/mol), obtained by MM-PBSA method, for curcumin and propafenone. Table S2: list of residues that have high probability to form contact with ligand. Tables S3–S7: names and types of atoms, masses, and charges used in the simulation of eterilate, itopride, propafenone, FSC, and curcumin, respectively, by Gromos96 43a1 force field ([PDF](#))

Movement of propafenone inside fibril during the 25 ns MD simulation ([AVI](#))

## ■ AUTHOR INFORMATION

### Corresponding Authors

\*E-mail: [masli@ifpan.edu.pl](mailto:masli@ifpan.edu.pl). Phone: +48 22 843 66 01 (M.S.L.).

\*E-mail: [chen15@mmc.edu.tw](mailto:chen15@mmc.edu.tw). Phone: +886-2-26363030 no. 1234 (Y.-C.C.).

### Author Contributions

S.T.N., S.-T.F., M.S.L., and Y.-C.C. conceived the experiments. S.T.N., S.-T.F., S.-H.H., C.-L.C., and P.D.Q.H. conducted the experiments. S.T.N., S.-T.F., P.D.Q.H., M.S.L., and Y.-C.C. analyzed the results. S.T.N., M.S.L., and Y.-C.C. wrote the paper. All authors reviewed the manuscript.

### Author Contributions

<sup>†</sup>S.T.N. and S.-T.F. have contributed equally.

### Funding

This work was supported by Department of Science and Technology at Ho Chi Minh city, Vietnam, Vietnam National Foundation for Science and Technology Development (NAFOSTED), under grant number 106-YS.02-2013.01 and by grants from Ministry of Science and Technology of Taiwan (NSC102-2627-M-715-002 and MOST103-2627-M-715-001 to Y.-C.C.) and grants from Mackay Medical College (1031B06 to Y.-C.C.).

### Notes

The authors declare no competing financial interest.

## ■ ACKNOWLEDGMENTS

The authors would like to thank the Department of Science and Technology at Ho Chi Minh City, Vietnam. Allocation of CPU time at the supercomputer center TASK in Gdansk (Poland) is highly appreciated.

## ■ REFERENCES

- (1) Henderson, A. S.; Jorm, A. F.: *Dementia*; John Wiley & Sons Ltd, 2002.
- (2) Nasica-Labouze, J.; Nguyen, P. H.; Sterpone, F.; Berthoumieu, O.; Buchete, N. V.; Cote, S.; De Simone, A.; Doig, A. J.; Faller, P.; Garcia, A.; Laio, A.; Li, M. S.; Melchionna, S.; Mousseau, N.; Mu, Y. G.; Paravastu, A.; Pasquali, S.; Rosenman, D. J.; Strodel, B.; Tarus, B.; Viles, J. H.; Zhang, T.; Wang, C. Y.; Derreumaux, P. Amyloid beta Protein and Alzheimer's Disease: When Computer Simulations Complement Experimental Studies. *Chem. Rev.* **2015**, *115*, 3518–3563.
- (3) Greene, J. D. W.; Baddeley, A. D.; Hodges, J. R. Analysis of the Episodic Memory Deficit in Early Alzheimers Disease: Evidence from the Doors and People Test. *Neuropsychologia* **1996**, *34*, 537–551.
- (4) Price, B. H.; Gurvit, H.; Weintraub, S.; Geula, C.; Leimkuhler, E.; Mesulam, M. Neuropsychological Patterns and Language Deficits in 20 Consecutive Cases of Autopsy-confirmed Alzheimer's Disease. *Arch. Neurol.* **1993**, *50*, 931–937.
- (5) Esteban-Santillan, C.; Praditswan, R.; Veda, H.; Geldmacher, D. S. Clock Drawing Test in Very Mild Alzheimer's Disease. *J. Am. Geriatr. Soc.* **1998**, *46*, 1266–1269.
- (6) Hardy, J.; Selkoe, D. J. Medicine - The Amyloid Hypothesis of Alzheimer's Disease: Progress and Problems on the Road to Therapeutics. *Science* **2002**, *297*, 353–356.
- (7) Citron, M. Strategies for Disease Modification in Alzheimer's Disease. *Nat. Rev. Neurosci.* **2004**, *5*, 677–685.
- (8) Li, H. Y.; Monien, M. B.; Lomakin, A.; Zemel, R.; Fradinger, E. A.; Tan, M. A.; Spring, S. M.; Urbanc, B.; Xie, C. W.; Benedek, G. B.; Bitan, G. Mechanistic Investigation of the Inhibition of A beta 42 Assembly and Neurotoxicity by A beta 42 C-terminal. *Biochemistry* **2010**, *49*, 6358–6364.
- (9) Wu, C.; Murray, M. M.; Bernstein, S. L.; Condron, M. M.; Bitan, G.; Shea, J. E.; Bowers, M. T. The Structure of A beta 42 C-Terminal Fragments Probed by a Combined Experimental and Theoretical Study. *J. Mol. Biol.* **2009**, *387*, 492–501.
- (10) Tjernberg, L. O.; Naslund, J.; Lindqvist, F.; Johansson, J.; Karlstrom, A. R.; Thyberg, J.; Terenius, L.; Nordstedt, C. Arrest of Beta-amyloid Peptide Fibril Formation by a Pentapeptide. *J. Biol. Chem.* **1996**, *271*, 8545–8548.

- (11) Ngo, S. T.; Li, M. S. Top-leads from Natural Products for Treatment of Alzheimer's Disease: Docking and Molecular Dynamics Study. *Mol. Simul.* **2013**, *39*, 279–291.
- (12) Viet, M. H.; Chen, C. Y.; Hu, C. K.; Chen, Y. R.; Li, M. S. Discovery of Dihydrochalcone as Potential Lead for Alzheimer's Disease: In Silico and In Vitro Study. *PLoS One* **2013**, *8*, e79151.
- (13) Yang, F. S.; Lim, G. P.; Begum, A. N.; Ubeda, O. J.; Simmons, M. R.; Ambegaokar, S. S.; Chen, P. P.; Kayed, R.; Glabe, C. G.; Frautschy, S. A.; Cole, G. M. Curcumin Inhibits Formation of Amyloid beta Oligomers and Fibrils, Binds Plaques, and Reduces Amyloid in vivo. *J. Biol. Chem.* **2005**, *280*, 5892–5901.
- (14) Ngo, S. T.; Li, M. S. Curcumin Binds to Abeta1–40 Peptides and Fibrils Stronger than Ibuprofen and Naproxen. *J. Phys. Chem. B* **2012**, *116*, 10165–10175.
- (15) Huy, P. D. Q.; Yu, Y.-C.; Ngo, S. T.; Thao, T. V.; Chen, C.-P.; Li, M. S.; Chen, Y.-C. In silico and in vitro Characterization of Anti-amyloidogenic Activity of Vitamin K3 Analogue for Alzheimer's Disease. *Biochim. Biophys. Acta, Gen. Subj.* **2013**, *1830*, 2960–2969.
- (16) Madrid, P. B.; Chopra, S.; Manger, I. D.; Gilfillan, L.; Keepers, T. R.; Shurtleff, A. C.; Green, C. E.; Iyer, L. V.; Dilks, H. H.; Davey, R. A.; Kolokoltsov, A. A.; Carrion, R.; Patterson, J. L.; Bavari, S.; Panchal, R. G.; Warren, T. K.; Wells, J. B.; Moos, W. H.; Burke, R. L.; Tanga, M. J. A Systematic Screen of FDA-Approved Drugs for Inhibitors of Biological Threat Agents. *PLoS One* **2013**, *8*, e60579.
- (17) Coskuner, O.; Murray, I. V. J. Adenosine Triphosphate (ATP) Reduces Amyloid-beta Protein Misfolding in vitro. *J. Alzheimers Dis.* **2014**, *41*, 561–574.
- (18) Wang, J.; Ono, K.; Dickstein, D. L.; Arrieta-Cruz, I.; Zhao, W.; Qian, X. J.; Lamparello, A.; Subnani, R.; Ferruzzi, M.; Pavlides, C.; Ho, L.; Hof, P. R.; Teplow, D. B.; Pasinetti, G. M. Carvedilol as a Potential Novel Agent for the Treatment of Alzheimer's Disease. *Neurobiol. Aging* **2011**, *32*, 32321.e1.
- (19) Paris, D.; Quadros, A.; Humphrey, J.; Patel, N.; Crescentini, R.; Crawford, F.; Mullan, M. Nilvadipine Antagonizes both A beta Vasoactivity in Isolated Arteries, and the Reduced Cerebral Blood Flow in APPsw Transgenic Mice. *Brain Res.* **2004**, *999*, 53–61.
- (20) Varea, S. ATP in Alzheimer Disease. National Library of Medicine (US), Bethesda (MD), <https://clinicaltrials.gov/ct2/show/NCT02279511> (accessed October 22 2014).
- (21) Johns Hopkins University; Mount Sinai School of Medicine. Trial of Carvedilol in Alzheimer's Disease. National Library of Medicine (US), Bethesda (MD), <https://clinicaltrials.gov/show/NCT01354444> (accessed May 9 2011).
- (22) Lawlor, B. A Phase III Trial of Nilvadipine to Treat Alzheimer's Disease (NILVAD). National Library of Medicine (US), Bethesda (MD), <https://clinicaltrials.gov/ct2/show/NCT02017340> (accessed December 16 2013).
- (23) Porat, Y.; Abramowitz, A.; Gazit, E. Inhibition of Amyloid Fibril Formation by Polyphenols: Structural Similarity and Aromatic Interactions as a Common Inhibition Mechanism. *Chem. Biol. Drug Des.* **2006**, *67*, 27–37.
- (24) Park, S. Y.; Kim, H. S.; Cho, E. K.; Kwon, B. Y.; Phark, S.; Hwang, K. W.; Sul, D. Curcumin Protected PC12 Cells against Beta-Amyloid-Induced Toxicity through the Inhibition of Oxidative Damage and Tau Hyperphosphorylation. *Food Chem. Toxicol.* **2008**, *46*, 2881–2887.
- (25) Zhang, L.; Fiala, M.; Cashman, J.; Sayre, J.; Espinosa, A.; Mahanian, M.; Zaghi, J.; Badmaev, V.; Graves, M. C.; Bernard, G.; Rosenthal, M. Curcuminoids Enhance Amyloid-beta Uptake by Macrophages of Alzheimer's Disease Patients. *J. Alzheimers Dis.* **2006**, *10*, 1–7.
- (26) Frautschy, S. A.; Hu, W.; Kim, P.; Miller, S. A.; Chu, T.; Harris-White, M. E.; Cole, G. M. Phenolic Anti-inflammatory Antioxidant Reversal of A beta-induced Cognitive Deficits and Neuropathology. *Neurobiol. Aging* **2001**, *22*, 993–1005.
- (27) Ringman, J. M.; Frautschy, S. A.; Teng, E.; Begum, A. N.; Bardens, J.; Beigi, M.; Gylys, K. H.; Badmaev, V.; Heath, D. D.; Apostolova, L. G.; Porter, V.; Vanek, Z.; Marshall, G. A.; Hellermann, G.; Sugar, C.; Masterman, D. L.; Montine, T. J.; Cummings, J. L.; Cole, G. M. Oral Curcumin for Alzheimer's Disease: Tolerability and Efficacy in a 24-week Randomized, Double Blind, Placebo-Controlled Study. *Alzheimer's Res. Ther.* **2012**, *4*, 43.
- (28) Baum, L.; Lam, C. W. K.; Cheung, S. K. K.; Kwok, T.; Lui, V.; Tsoh, J.; Lam, L.; Leung, V.; Hui, E.; Ng, C.; Woo, J.; Chiu, H. F. K.; Goggins, W. B.; Zee, B. C. Y.; Cheng, K. F.; Fong, C. Y. S.; Wong, A.; Mok, H.; Chow, M. S. S.; Ho, P. C.; Ip, S. P.; Ho, C. S.; Yu, X. W.; Lai, C. Y. L.; Chan, M. H.; Szeto, S.; Chan, I. H. S.; Mok, V. Six-month Randomized, Placebo-controlled, Double-blind, Pilot Clinical Trial of Curcumin in Patients with Alzheimer's Disease. *J. Clin. Psychopharmacol.* **2008**, *28*, 110–113.
- (29) Small-Molecule Drug Discovery Suite 2010, QikProp, version 3.3; Schrödinger, L. L. C.: New York, N.Y., 2010.
- (30) Yang, J.; Chen, J. QSAR Analysis of Purine-Type and Propafenone-Type Substrates of P-Glycoprotein Targeting  $\beta$ -Amyloid Clearance. *Neurodegenerative Diseases* **2013**, DOI: [10.5772/S4975](https://doi.org/10.5772/S4975).
- (31) Ryu, E. K.; Choe, Y. S.; Lee, K. H.; Choi, Y.; Kim, B. T. Curcumin and Dehydrozingerone Derivatives: Synthesis, Radio-labeling, and Evaluation for Beta-Amyloid Plaque Imaging. *J. Med. Chem.* **2006**, *49*, 6111–6119.
- (32) Ngo, S. T.; Mai, B. K.; Hiep, D. M.; Li, M. S. Estimation of the Binding Free Energy of AC1INX476 to HIV-1 Protease Wild Type and Mutations Using FreeEnergy Perturbation Method. *Chem. Biol. Drug Des.* **2015**, *86*, 546–558.
- (33) Jayachandran, G.; Shirts, M. R.; Park, S.; Pande, V. S. Parallelized-over-parts Computation of Absolute Binding Free Energy with Docking and Molecular Dynamics. *J. Chem. Phys.* **2006**, *125*, 084901.
- (34) Bennett, C. H. Efficient Estimation of Free Energy Differences from Monte Carlo Data. *J. Comput. Phys.* **1976**, *22*, 245–268.
- (35) Roychaudhuri, R.; Yang, M.; Hoshi, M. M.; Teplow, D. B. Amyloid beta-Protein Assembly and Alzheimer Disease. *J. Biol. Chem.* **2009**, *284*, 4749–4753.
- (36) Bernstein, S. L.; Dupuis, N. F.; Lazo, N. D.; Wyttenbach, T.; Condron, M. M.; Bitan, G.; Teplow, D. B.; Shea, J. E.; Ruotolo, B. T.; Robinson, C. V.; Bowers, M. T. Amyloid-beta Protein Oligomerization and the Importance of Tetramers and Dodecamers in the Etiology of Alzheimer's Disease. *Nat. Chem.* **2009**, *1*, 326–331.
- (37) Harper, J. D.; Wong, S. S.; Lieber, C. M.; Lansbury, P. T. Observation of Metastable A beta Amyloid Protofibrils by Atomic Force Microscopy. *Chem. Biol.* **1997**, *4*, 119–125.
- (38) Demuro, A.; Mina, E.; Kayed, R.; Milton, S. C.; Parker, I.; Glabe, C. G. Calcium Dysregulation and Membrane Disruption as a Ubiquitous Neurotoxic Mechanism of Soluble Amyloid Oligomers. *J. Biol. Chem.* **2005**, *280*, 17294–17300.
- (39) Chebaro, Y.; Jiang, P.; Zang, T.; Mu, Y. G.; Nguyen, P. H.; Mousseau, N.; Derreumaux, P. Structures of A beta 17–42 Trimmers in Isolation and with Five Small-Molecule Drugs Using a Hierarchical Computational Procedure. *J. Phys. Chem. B* **2012**, *116*, 8412–8422.
- (40) Zhang, T.; Zhang, J.; Derreumaux, P.; Mu, Y. G. Molecular Mechanism of the Inhibition of EGCG on the Alzheimer A beta(1–42) Dimer. *J. Phys. Chem. B* **2013**, *117*, 3993–4002.
- (41) Doig, A. J.; Derreumaux, P. Inhibition of Protein Aggregation and Amyloid Formation by Small Molecules. *Curr. Opin. Struct. Biol.* **2015**, *30*, 50–56.
- (42) Jiang, P.; Li, W. F.; Shea, J. E.; Mu, Y. G. Resveratrol Inhibits the Formation of Multiple-Layered beta-Sheet Oligomers of the Human Islet Amyloid Polypeptide Segment 22–27. *Biophys. J.* **2011**, *100*, 1550–1558.
- (43) Luhrs, T.; Ritter, C.; Adrian, M.; Riek-Lohr, D.; Bohrmann, B.; Dobeli, H.; Schubert, D.; Riek, R. 3D Structure of Alzheimer's Amyloid-beta(1–42) Fibrils. *Proc. Natl. Acad. Sci. U. S. A.* **2005**, *102*, 17342–17347.
- (44) Petkova, A. T.; Yau, W. M.; Tycko, R. Experimental Constraints on Quaternary Structure in Alzheimer's Beta-Amyloid Fibrils. *Biochemistry* **2006**, *45*, 498–512.
- (45) Paravastu, A. K.; Leapman, R. D.; Yau, W. M.; Tycko, R. Molecular Structural Basis for Polymorphism in Alzheimer's Beta-amyloid Fibrils. *Proc. Natl. Acad. Sci. U. S. A.* **2008**, *105*, 18349–18354.

- (46) Lu, J. X.; Qiang, W.; Yau, W. M.; Schwieters, C. D.; Meredith, S. C.; Tycko, R. Molecular Structure of beta-Amyloid Fibrils in Alzheimer's Disease Brain Tissue. *Cell* **2013**, *154*, 1257–1268.
- (47) Viet, M. H.; Ngo, S. T.; Lam, N. S.; Li, M. S. Inhibition of Aggregation of Amyloid Peptides by Beta-Sheet Breaker Peptides and Their Binding Affinity. *J. Phys. Chem. B* **2011**, *115*, 7433–7446.
- (48) Viet, M. H.; Siposova, K.; Bednarikova, Z.; Antosova, A.; Nguyen, T. T.; Gazova, Z.; Li, M. S. In Silico and in Vitro Study of Binding Affinity of Tripeptides to Amyloid beta Fibrils: Implications for Alzheimer's Disease. *J. Phys. Chem. B* **2015**, *119*, 5145–5155.
- (49) Bhavaraju, M.; Phillips, M.; Bowman, D.; Aceves-Hernandez, J. M.; Hansmann, U. H. E. Binding of ACE-inhibitors to in Vitro and Patient-Derived Amyloid-beta Fibril Models. *J. Chem. Phys.* **2016**, *144*, 015101.
- (50) Lemkul, J. A.; Bevan, D. R. The Role of Molecular Simulations in the Development of Inhibitors of Amyloid beta-Peptide Aggregation for the Treatment of Alzheimer's Disease. *ACS Chem. Neurosci.* **2012**, *3*, 845–856.
- (51) Butterfield, D. A.; Reed, T.; Newman, S. F.; Sultana, R. Roles of Amyloid Beta-Peptide-Associated Oxidative Stress and Brain Protein Modifications in the Pathogenesis of Alzheimer's Disease and Mild Cognitive Impairment. *Free Radical Biol. Med.* **2007**, *43*, 658–677.
- (52) Yatin, S. M.; Varadarajan, S.; Link, C. D.; Butterfield, D. A. In vitro and in vivo Oxidative Stress Associated with Alzheimer's Amyloid Beta-Peptide (1–42). *Neurobiol. Aging* **1999**, *20*, 325–330.
- (53) Lee, V. M. Y. Amyloid Binding Ligands as Alzheimer's Disease Therapies. *Neurobiol. Aging* **2002**, *23*, 1039–1042.
- (54) Nie, Q.; Du, X. G.; Geng, M. Y. Small Molecule Inhibitors of Amyloid Beta Peptide Aggregation as a Potential Therapeutic Strategy for Alzheimer's Disease. *Acta Pharmacol. Sin.* **2011**, *32*, 545–551.
- (55) Kolstoe, S. E.; Wood, S. P. Drug Targets for Amyloidosis. *Biochem. Soc. Trans.* **2010**, *38*, 466–470.
- (56) Willett, P.; Barnard, J. M.; Downs, G. M. Chemical Similarity Searching. *J. Chem. Inf. Comput. Sci.* **1998**, *38*, 983–996.
- (57) Hamelberg, D.; McCammon, J. A. Standard Free Energy of Releasing a Localized Water Molecule from the Binding Pockets of Proteins: Double-Decoupling Method. *J. Am. Chem. Soc.* **2004**, *126*, 7683–7689.
- (58) Nguyen, T. T.; Mai, B. K.; Li, M. S. Study of Tamiflu Sensitivity to Variants of A/HSN1 Virus Using Different Force Fields. *J. Chem. Inf. Model.* **2011**, *51*, 2266–2276.
- (59) Hou, T. J.; Wang, J. M.; Li, Y. Y.; Wang, W. Assessing the Performance of the MM/PBSA and MM/GBSA Methods. 1. The Accuracy of Binding Free Energy Calculations Based on Molecular Dynamics Simulations. *J. Chem. Inf. Model.* **2011**, *51*, 69–82.
- (60) Viet, M. H.; Ngo, S. T.; Lam, N. S.; Li, M. S. Inhibition of Aggregation of Amyloid Peptides by Beta-Sheet Breaker Peptides and Their Binding Affinity. *J. Phys. Chem. B* **2011**, *115*, 7433–7446.
- (61) Joosten, R. P.; te Beek, T.; Krieger, E.; Hekkelman, M. L.; Hooft, R. W. W.; Schneider, R.; Sander, C.; Vriend, G. A Series of PDB Related Databases for Everyday Needs. *Nucleic Acids Res.* **2011**, *39*, D411–D419.
- (62) Kabsch, W.; Sander, C. Dictionary of Protein Secondary Structure - Pattern-Recognition of Hydrogen-Bonded and Geometrical Features. *Biopolymers* **1983**, *22*, 2577–2637.
- (63) Wang, J.; Zhang, Y. J.; Du, S. The Protective Effect of Curcumin on A beta Induced Aberrant Cell Cycle Reentry on Primary Cultured Rat Cortical Neurons. *Eur. Rev. Med. Pharmacol. Sci.* **2012**, *16*, 445–454.
- (64) Berthoumieu, O.; Nguyen, P. H.; del Castillo-Frias, M. P.; Ferre, S.; Tarus, B.; Nasica-Labouze, J.; Noel, S.; Saurel, O.; Rampon, C.; Doig, A. J.; Derreumaux, P.; Faller, P. Combined Experimental and Simulation Studies Suggest a Revised Mode of Action of the Anti-Alzheimer Disease Drug NQ-Trp. *Chem. - Eur. J.* **2015**, *21*, 12657–12666.
- (65) Liao, M. Q.; Tzeng, Y. J.; Chang, L. Y. X.; Huang, H. B.; Lin, T. H.; Chyan, C. L.; Chen, Y. C. The Correlation between Neurotoxicity, Aggregative Ability and Secondary Structure Studied by Sequence Truncated A beta Peptides. *FEBS Lett.* **2007**, *581*, 1161–1165.
- (66) Holliday, J. D.; Ranade, S. S.; Willett, P. A Fast Algorithm for Selecting Sets of Dissimilar Molecules from Large Chemical Databases. *Quant. Struct.-Act. Relat.* **1995**, *14*, 501–506.
- (67) Barreiro, G.; Guimaraes, C. R. W.; Tubert-Brohman, I.; Lyons, T. M.; Tirado-Rives, J.; Jorgensen, W. L. Search for Non-nucleoside Inhibitors of HIV-1 Reverse Transcriptase Using Chemical Similarity, Molecular Docking, and MM-GB/SA Scoring. *J. Chem. Inf. Model.* **2007**, *47*, 2416–2428.
- (68) Wang, Y. L.; Xiao, J. W.; Suzek, T. O.; Zhang, J.; Wang, J. Y.; Zhou, Z. G.; Han, L. Y.; Karapetyan, K.; Dracheva, S.; Shoemaker, B. A.; Bolton, E.; Gindulyte, A.; Bryant, S. H. PubChem's BioAssay Database. *Nucleic Acids Res.* **2012**, *40*, D400–D412.
- (69) Sanner, M. F. Python: A Programming Language for Software Intergration and Development. *J. Mol. Graphics Modell.* **1999**, *17*, 57–61.
- (70) Trott, O.; Olson, A. J. Improving the Speed and Accuracy of Docking with a New Scoring Function, Efficient Optimization, and Multithreading. *J. Comput. Chem.* **2010**, *31*, 455–461.
- (71) Shanno, D. F. Conditioning of Quasi-Newton Methods for Function Minimization. *Math. Comput.* **1970**, *24*, 647–656.
- (72) Morris, G. M.; Goodsell, D. S.; Halliday, R. S.; Huey, R.; Hart, W. E.; Belew, R. K.; Olson, A. J. Automated Docking Using a Lamarckian Genetic Algorithm and an Empirical Binding Free Energy Function. *J. Comput. Chem.* **1998**, *19*, 1639–1662.
- (73) Morris, G. M.; Goodsell, D. S.; Huey, R.; Olson, A. J. Distributed Automated Docking of Flexible Ligands to Proteins: Parallel Applications of AutoDock 2.4. *J. Comput.-Aided Mol. Des.* **1996**, *10*, 293–304.
- (74) Hess, B.; Kutzner, C.; van der Spoel, D.; Lindahl, E. Gromacs 4: Algorithms for Highly Efficient, Load-Balanced, and Scalable Molecular Simulation. *J. Chem. Theory Comput.* **2008**, *4*, 435–447.
- (75) van Gunsteren, W. F.; Billeter, S. R.; Eising, A. A.; Hunenberger, P. H.; Kruger, P.; Mark, A. E.; Scott, W. R. P.; Tironi, I. G. *Biomolecular Simulation: The GROMOS96 Manual and User Guide*; Vdf Hochschulverlag AG an der ETH: Zurich, 1996.
- (76) Scott, W. R. P.; Hunenberger, P. H.; Tironi, I. G.; Mark, A. E.; Billeter, S. R.; Fennen, J.; Torda, A. E.; Huber, T.; Krüger, P.; van Gunsteren, W. F. The GROMOS Biomolecular Simulation Program Package. *J. Phys. Chem. A* **1999**, *103*, 3596–3607.
- (77) Berendsen, H. J. C.; Postma, J. P. M.; van Gunsteren, W. F.; Hermans, J. *Intermolecular Forces*; Reidel: Dordrecht, 1981.
- (78) Schuttekkopf, A. W.; van Aalten, D. M. F. PRODRG: a Tool for High-Throughput Crystallography of Protein-Ligand Complexes. *Acta Crystallogr., Sect. D: Biol. Crystallogr.* **2004**, *60*, 1355–1363.
- (79) Bayly, C. I.; Cieplak, P.; Cornell, W.; Kollman, P. A. A Well-Behaved Electrostatic Potential Based Method Using Charge Restraints for Deriving Atomic Charges: the RESP Model. *J. Phys. Chem.* **1993**, *97*, 10269–10280.
- (80) Hess, B.; Bekker, H.; Berendsen, H. J. C.; Fraaije, J. G. E. M. LINCS: A Linear Constraint Solver for Molecular Simulations. *J. Comput. Chem.* **1997**, *18*, 1463–1472.
- (81) Darden, T.; York, D.; Pedersen, L. Particle Mesh Ewald: An N-log(N) Method for Ewald Sums in Large Systems. *J. Chem. Phys.* **1993**, *98*, 10089–10092.
- (82) Zwanzig, R. W. High-Temperature Equation of State by a Perturbation Method. I. Nonpolar Gases. *J. Chem. Phys.* **1954**, *22*, 1420–1426.
- (83) Fujitani, H.; Tanida, Y.; Ito, M.; Jayachandran, G.; Snow, C. D.; et al. Direct Calculation of the Binding Free Energies of FKBP Ligands. *J. Chem. Phys.* **2005**, *123*, 084108.
- (84) Kollman, P. A.; Massova, I.; Reyes, C.; Kuhn, B.; Huo, S.; Chong, L.; Lee, M.; Lee, T.; Duan, Y.; Wang, W.; Donini, O.; Cieplak, P.; Srinivasan, J.; Case, D. A.; Cheatham, I. Calculating Structures and Free Energies of Complex Molecules: Combining Molecular Mechanics and Continuum Models. *Acc. Chem. Res.* **2000**, *33*, 889–897.
- (85) McQuarrie, D. A. *Statistical Thermodynamics*; Harper and Row: New York, 1973.

- (86) Shrake, A.; Rupley, J. A. Environment and Exposure to Solvent of Protein Atoms-Lysozyme and Insulin. *J. Mol. Biol.* **1973**, *79*, 351–371.
- (87) Baker, N. A.; Sept, D.; Joseph, S.; Holst, M. J.; McCammon, J. A. Electrostatics of Nanosystems: Application to Microtubules and the Ribosome. *Proc. Natl. Acad. Sci. U. S. A.* **2001**, *98*, 10037–10041.
- (88) Sitkoff, D.; Sharp, K. A.; Honig, B. Accurate Calculation of Hydration Free Energies Using Macroscopic Solvent Models. *J. Phys. Chem.* **1994**, *98*, 1978–1988.
- (89) Opazo, C.; Huang, X. D.; Cherny, R. A.; Moir, R. D.; Roher, A. E.; White, A. R.; Cappai, R.; Masters, C. L.; Tanzi, R. E.; Inestrosa, N. C.; Bush, A. I. Metalloenzyme-like Activity of Alzheimer's Disease Beta-Amyloid - Cu-dependent Catalytic Conversion of Dopamine, Cholesterol, and Biological Reducing Agents to Neurotoxic H<sub>2</sub>O<sub>2</sub>. *J. Biol. Chem.* **2002**, *277*, 40302–40308.